Escape from pinch-off during contraction of liquid sheets and two-dimensional drops of low-viscosity fluids

Hansol Wee, Ajay Harishankar Kumar, Xiao Liu, and Osman A. Basaran*
Davidson School of Chemical Engineering, Purdue University, West Lafayette, Indiana 47907, USA

(Received 17 May 2024; accepted 11 September 2024; published 9 October 2024)

Liquid sheets are omnipresent in nature and applications. The cross sections of liquid sheets are elongated two-dimensional (2D) drops the two ends of which contract towards each other because of surface tension (σ). If sufficiently thin, sheets can rupture due to van der Waals forces. Burton and Taborek, however, have shown that regardless of sheet thickness $2\tilde{h}_0$, a contracting inviscid liquid sheet can break even in their absence. Here we use 2D simulations and theory to show that for small yet finite viscosity μ, contracting liquid sheets will escape from pinch-off when van der Waals forces are absent due surprisingly to two distinct mechanisms that depend on Ohnseorge number $\mathrm{Oh} = \mu/\sqrt{\rho\sigma\tilde{h}_0}$ (ρ: density). For $\mathrm{Oh} \to 0$, escape is shown to be due to viscous resistance, while for larger but yet still small Oh, it can be attributed to vorticity generation at the free surface. The distinct mechanisms yield different scaling laws relating minimum sheet thickness when escape occurs to Oh.

DOI: 10.1103/PhysRevFluids.9.103601

I. INTRODUCTION

Liquid sheets that are surrounded by a gas are encountered in daily life in water falls and fountains and in diverse industrial settings including ones where liquid is ejected from a spray nozzle [1,2] and extruded from a die in polymer processing [3]. In all but the last example, the sheets eventually disintegrate into drops. In contrast to a cylindrical liquid jet that is destabilized by surface tension and disintegrates into drops [4,5], a quiescent liquid sheet of uniform thickness $2\tilde{h}_0$ that is of indefinitely large lateral extent is linearly stable if $2\tilde{h}_0$ is much larger than a micrometer. Because of surface tension, any sinusoidal perturbation to the surface of the sheet causes the pressure to rise where the interface forms peaks and to fall where it forms valleys, leading fluid to flow from regions where interface height is elevated to ones where it is depressed, thereby resulting in the sheet to return to its flat configuration. When $2\tilde{h}_0$ is of the order of micrometers or smaller [6,7], liquid sheets are linearly unstable due to intermolecular van der Waals forces and can disintegrate spontaneously [8–11]. The dynamics in the final stages of thinning as a liquid sheet approaches rupture is self-similar: For Newtonian fluids, it has been shown by Vaynblat *et al.* [12] that the self-similarity is of the first kind [13] and that inertia and viscous and van der Waals forces grow without bound as sheet thickness tends to zero and the rupture singularity is approached. Since the pioneering work of Vaynblat *et al.* [12], the dynamics of sheet rupture has received much attention, including studies that have considered breakup sheets of slightly and highly viscous Newtonian fluids [14,15] as well as that of complex fluids [16–19].

In practice, cross sections of sheets resemble elongated two-dimensional (2D) drops: They are virtually rectangular in shape albeit for their two rounded ends. Because of surface tension (σ), the capillary pressure $\sigma/\tilde{h}_0$ in the two semicircular ends is larger than that in the flat slender body

*Contact author: obasaran@purdue.edu

of the 2D drop where it equals zero. This capillary pressure difference causes the two ends of the 2D drop to contract toward each other. The contraction dynamics of 2D sheets has received much attention since Taylor and Culick [20,21] deduced the speed with which the edges of such sheets retract [22–25]. Moreover, Burton and Taborek [26] have shown that regardless of sheet thickness $2\tilde{h}_0$, a contracting inviscid liquid sheet can pinch off even in the absence of van der Waals forces. The pinch-off dynamics exhibits self-similarity of the second kind [13] with irrational scaling exponents. Recently, it has been shown in Ref. [27] that when fluid viscosity is nonzero, a sheet cannot spontaneously rupture unless an external force is applied.

In this paper, we use simulation and theory to show that for small yet finite viscosity μ, contracting liquid sheets and 2D drops will escape from breakup when van der Waals forces are absent due surprisingly to two distinct mechanisms that depend on Ohnseorge number $\mathrm{Oh} = \mu/\sqrt{\rho\sigma\tilde{h}_0}$ (ρ: density). For $\mathrm{Oh} \to 0$, escape is shown to be due to viscous resistance in a thinning sheet that ultimately becomes important no matter how small the fluid's viscosity, while for larger but yet still small Oh, it can be attributed to vorticity generation at the highly curved free surface. We also show that the distinct mechanisms yield different scaling laws relating minimum sheet thickness when escape occurs to Oh.

The paper is organized as follows. Section II presents the mathematical statement of the problem. In this paper, the thinning of liquid sheets and 2D drops is analyzed by solving both the full free surface flow problem governed by the continuity and Navier-Stokes equations in 2D (Sec. II) and also a set of slender-sheet equations in 1D (Sec. III). The simulation techniques used to solve both are summarized in Sec. IV. Results obtained from 2D simulations are presented in Sec. V followed by ones from 1D simulations in Sec. VI. The paper concludes with a summary of key results and recommendations for some possible avenues of future work in Sec. VII.

II. PROBLEM FORMULATION

The system is isothermal and consists of a liquid sheet of an incompressible Newtonian fluid of density ρ and viscosity μ that is surrounded by a dynamically passive gas [Fig. 1(a)]. The surface tension of the interface separating the sheet from the surroundings is denoted by σ. It proves convenient to use a Cartesian coordinate system $(\tilde{x}, \tilde{y}, \tilde{z})$, with the $\tilde{x}$ axis pointing along the neutral direction in which the sheet is indefinitely long or the system is translationally symmetric. Initially, the intersection of planes that are parallel to the $\tilde{y}\tilde{z}$ plane with the sheet resemble slender 2D drops, with their top and bottom surfaces located at $\tilde{y} = \pm\tilde{h}_0$. The 2D drops are terminated by semicircular ends each of radius $\tilde{h}_0$ and are of length $2\tilde{L}_0$ in the $\tilde{z}$ direction [Fig. 1(b)]. With the origin of the coordinate system located along the line that passes through the centers of the 2D drops, i.e., the $\tilde{x}$ axis, the goal is to determine the evolution in time of the drop shape and the 2D flow within it in one quadrant of the $\tilde{y}\tilde{z}$ plane [Fig. 1(b)].

We nondimensionalize the problem using the initial sheet half-thickness $\tilde{h}_0$, the inertial-capillary time $\tilde{t}_{ic} \equiv \sqrt{\rho\tilde{h}_0^3/\sigma}$, and capillary pressure $\sigma/\tilde{h}_0$ as characteristic length, time, and stress scales. Henceforward, variables without tildes over them denote the dimensionless counterparts of those with tildes. The flow within a 2D drop is governed by the (dimensionless) continuity and Navier-Stokes equations

$$\nabla \cdot \mathbf{v} = 0, \tag{1}$$

$$\frac{D\mathbf{v}}{Dt} \equiv \frac{\partial \mathbf{v}}{\partial t} + \mathbf{v} \cdot \nabla\mathbf{v} = \nabla \cdot \mathbf{T}, \tag{2}$$

where $\mathbf{T} = -p\mathbf{I} + \mathrm{Oh}[(\nabla\mathbf{v}) + (\nabla\mathbf{v})^T]$. Here t is time, D/Dt the material derivative, $\mathbf{v}$ the fluid velocity, p the pressure, $\mathbf{T}$ the total stress tensor, and $\mathbf{I}$ the unit tensor.

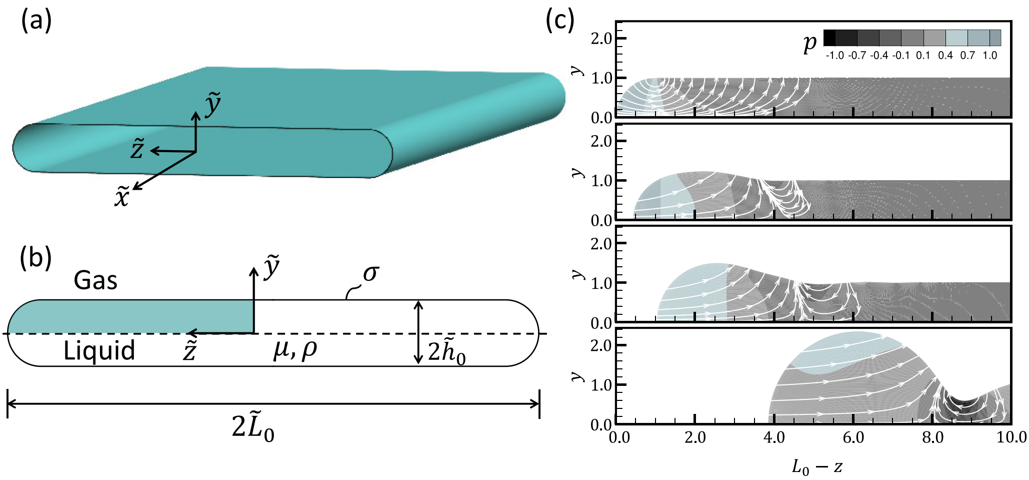

FIG. 1. Contraction of liquid sheets and 2D drops. (a) Definition sketch and coordinate system: An initially quiescent liquid sheet of uniform thickness with two rounded ends that is indefinitely long in the $\tilde{x}$ direction. (b) Cross sections of liquid sheets resemble elongated 2D drops. Because of symmetry, the problem domain, shaded in blue, is one quarter of the cross section. (c) Neck formation during the early stages of contraction. Computed profiles of and instantaneous streamlines and pressure contours within a contracting 2D drop of $\mathrm{Oh} = 5 \times 10^{-5}$ and $L_0 = 100$ at four instants in time: $t = 0.0255$ (topmost), $t = 1.215$ (second from the top), $t = 1.972$ (second from the bottom), and $t = 5.395$ (bottommost). The legend identifying the contour values of the pressure in the topmost subplot applies at all four instants.

The governing equations are solved subject to the kinematic and traction boundary conditions (BCs) at the interface $S(t)$. The former BC is

$$\mathbf{n} \cdot (\mathbf{v} - \mathbf{v}_I) = 0, \tag{3}$$

where $\mathbf{n}$ is the outward-pointing unit normal to $S(t)$ and $\mathbf{v}_I$ is the velocity of points on $S(t)$ while the latter BC is

$$\mathbf{n} \cdot \mathbf{T} = 2\mathcal{H}\mathbf{n}, \tag{4}$$

where $2\mathcal{H}$ stands for twice the mean curvature of $S(t)$ and the pressure in the gas surrounding the 2D drop is set equal to zero. Additionally, symmetry BCs are imposed on the flow field and the interface profile at $y = 0$ and $z = 0$. The problem statement is completed by specification of initial conditions (ICs) such that the 2D drop is released from a deformed state where the drop's initial aspect ratio is given by $L_0 \equiv \tilde{L}_0/\tilde{h}_0$ and the fluid within the drop is quiescent.

III. 1D SLENDER-SHEET EQUATIONS

When the sheet fluid is inviscid, Burton and Taborek [26] have shown that the dynamics in the vicinity of the space-time pinch-off singularity is not only self-similar but the interface shape is locally slender. Therefore, the local dynamics can be described by using the slender-sheet equations. In this limit, the 1D mass and momentum equations are [15,18,19,22,24]

$$\frac{\partial h}{\partial t} + \frac{\partial (hv)}{\partial z} = 0 \tag{5}$$

and

$$\frac{\partial v}{\partial t} + v\frac{\partial v}{\partial z} = \frac{\partial^3 h}{\partial z^3} + 4\frac{\mathrm{Oh}}{h}\frac{\partial}{\partial z}\left(h\frac{\partial v}{\partial z}\right), \tag{6}$$

where $y = h(z, t)$ denotes the local half-thickness of the sheet. In the slender limit, the lateral velocity is solely a function of the lateral coordinate z and time t, viz. $v = v(z, t)$, and the vertical velocity, which is small compared to the lateral velocity, is simply given by $u = -y\,\partial v/\partial z$.

In the 1D momentum equation, the left-hand side consists of the inertial terms while the first term on the right-hand side accounts for the contribution of the capillary pressure $-\partial^2 h/\partial z^2$ and the second term involving Oh accounts for the extensional viscous stress. Burton and Taborek [26] have solved Eqs. (5) and (6) when $\mathrm{Oh} = 0$. In Appendix A, we summarize the salient features of the self-similar dynamics when a liquid sheet of an inviscid fluid ruptures and also show how viscosity, no matter how small, modifies the inviscid dynamics.

In order to deal with the two tips of the 2D drop, as has been commonly done in the literature [22,28–30] the curvature term in (6) is replaced by its full counterpart $-\partial^2 h/\partial z^2/[1 + (\partial h/\partial z)^2]^{3/2}$ which reduces to $-\partial^2 h/\partial z^2$ in the slender portions of the 2D drop where $|\partial h/\partial z| \ll 1$. The dynamics of contraction of 2D drops is analyzed by solving the 1D slender-sheet equations (5) and (6) albeit with the expression for the full curvature. This system is augmented by a constraint that accounts for the fact that the volume (area) of the 2D drop is conserved. This integral constraint determines the instantaneous length $L(t)$ of the drop [31–33]. The evolution equations and the integral constraint are solved subject to the BCs that at the drop tip, $h = 0$ and the velocity of the drop's tip equals dL/dt, and that at $z = 0$, $\partial h/\partial z = 0$ and $v = 0$ because of symmetry. As in the 2D simulations, the fluid is taken to be quiescent initially in the 1D simulations.

IV. NUMERICAL METHODS

The free boundary problem consisting of the transient system of 2D continuity and Navier-Stokes equations subject to the aforementioned BCs and ICs in Sec. II is solved numerically by means of a fully implicit, arbitrary Lagrangian-Eulerian method-of-lines algorithm in which the Galerkin finite element method (G/FEM) is used for spatial discretization [34] and an adaptive, implicit finite difference method is employed for time integration [35,36]. As the thinning and possible rupture of a liquid sheet or 2D drop is a free boundary problem that involves a highly deformable liquid-gas interface, an elliptic mesh generation technique [37] is employed to track the moving boundary and determine the coordinates of each grid point in the moving, adaptive mesh simultaneously with the velocity and pressure unknowns in the sheet or 2D drop as well as the free surface profile. This algorithm is based on those described in Refs. [38–43] which have been used to solve diverse free surface flows with hydrodynamic singularities in situations involving multiphysics and multiscale dynamics.

The slender-sheet equations of Sec. III are solved by means of an algorithm in which the G/FEM is used for spatial discretization [34] and an adaptive, implicit finite difference method is employed for time integration [35,36]. The algorithm used here is based on those that have been used to analyze the dynamics of liquid bridges, thin liquid sheets and films, and dripping-jetting transitions in drop formation from a tube [18,28,29,44].

V. 2D RESULTS

Figure 1(c) shows results of simulations at early times in the immediate aftermath following the release of a low-viscosity 2D drop from a static deformation. The higher capillary pressure in the tip drives fluid from that region toward the flat portion of the drop where capillary pressure is zero and fluid is at rest. However, because of inertial resistance, fluid in the bulk of the drop cannot immediately begin to flow. Thus, the magnitude of the lateral velocity v decreases with increasing distance from the recoiling tip or $\partial v/\partial z < 0$. From the continuity equation, $\partial u/\partial y + \partial v/\partial z = 0$ (u: component of velocity in the vertical direction) and hence $\partial u/\partial y > 0$. Since $u = 0$ along the plane of symmetry $y = 0$, the vertical velocity must then increase with y from $y = 0$ to the free surface, causing the instantaneous streamlines to curve toward the free surface as shown in Fig. 1(c). Since $|\partial v/\partial z|$ and hence $|\partial u/\partial y|$ are larger for a streamline that starts from a higher value of y at the tip

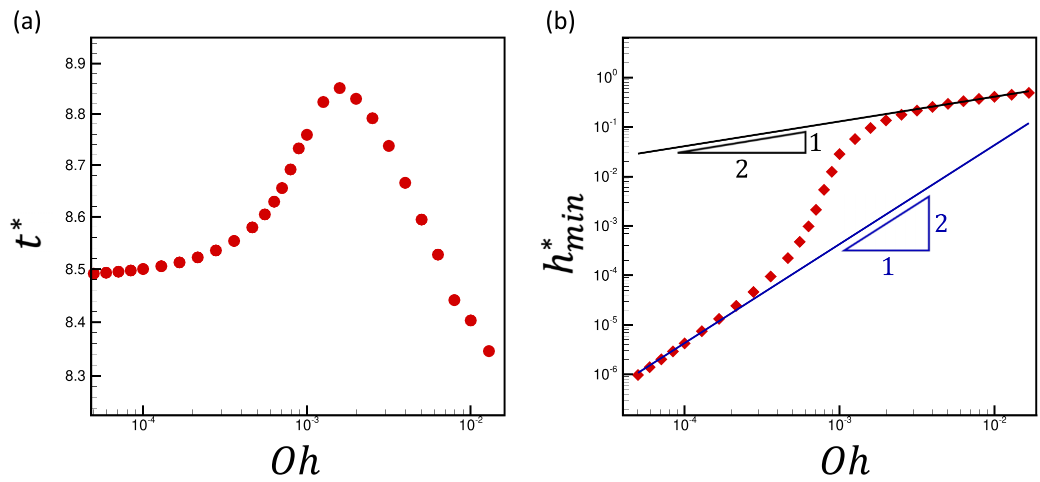

FIG. 2. The computed variation with Ohnesorge number Oh of (a) the time t^* and (b) the minimum value of the sheet half-thickness h^*_{min} at which the neck of a recoiling liquid sheet or a 2D drop stops thinning and the sheet escapes from pinch-off. Subplot (a) showing the variation of t^* with Oh indicates that there are two distinct types of response and hence two mechanisms behind the escape from pinch-off during contraction of slightly viscous liquid sheets. When $\mathrm{Oh} \to 0$ (for $\mathrm{Oh} < 2 \times 10^{-4}$ in the figure), the escape time is virtually unchanged as Oh varies. When $\mathrm{Oh} > 2 \times 10^{-3}$, t^* decreases as Oh increases because the rate at which vorticity generated at the free surface diffuses into and penetrates the pinching region increases with Oh. Subplot (b) showing the variation of h^*_{min} with Oh confirms the existence of the two different types of dynamical response and hence the two distinct mechanisms of escape from pinch-off. In the first region where $\mathrm{Oh} \to 0$, the simulation results (red diamonds) follow the theoretical scaling law $h^*_{\mathrm{min}} \sim \mathrm{Oh}^2$ (blue line of slope 2) and the escape is attributable to viscous resistance to further thinning of the neck, and in the second region where the Ohnesorge number is still small but not vanishingly so, viz. $\mathrm{Oh} \approx O(10^{-2})$, the simulation results (red diamonds) follow the theoretical scaling law $h^*_{\mathrm{min}} \sim \mathrm{Oh}^{1/2}$ (black line of slope 1/2) and the escape is due to vorticity in the recoiling 2D drop. Here $L_0 = 100$.

than one from a lower value of y, the tip of the drop begins to bulge out: Thus, because of mass conservation, a growing rim arises in the tip region and a thinning neck forms just downstream of the rim. Moreover, as seen in the last frame of Fig. 1(c), the resulting negative curvature of the free surface at the neck induces a flow in the positive z direction from the bulk of the drop far from the tip toward the vicinity of the neck. The collision of the flow driven from the retracting tip in the $-z$ direction with the flow driven from the previously quiescent bulk toward the tip results in additional thinning of the neck. As further discussed below, a self-accelerating process arises in which the magnitude of the velocity of the fluid being driven from the bulk toward the neck increases as the neck height decreases and the curvature at the neck becomes more negative, and the neck height decreases further as the magnitude of fluid velocity from the bulk through the neck increases. As shown by Burton and Taborek, in finite time the fluid velocity in the vicinity of the neck diverges and the 2D drop pinches off when the fluid is inviscid ($\mu = 0$ or $\mathrm{Oh} = 0$) even when van der Waals forces are absent.

Figure 2, however, shows that even a minute amount of viscosity will prevent pinch-off during retraction of sheets. After the elapse of time t^* from the beginning of contraction and when the minimum value of the sheet half-thickness h_{min} has fallen to an extremely small value $h^*_{\mathrm{min}} \ll 1$, the thickness of the sheet at the location where it is smallest no longer continues to decrease but instead h_{min} starts to increase and hence the neck begins to reopen. The results of Fig. 2 show that there are two distinct scaling regimes of escape from pinch-off when $\mathrm{Oh} \ll 1$: one as $\mathrm{Oh} \to 0$ where t^* does

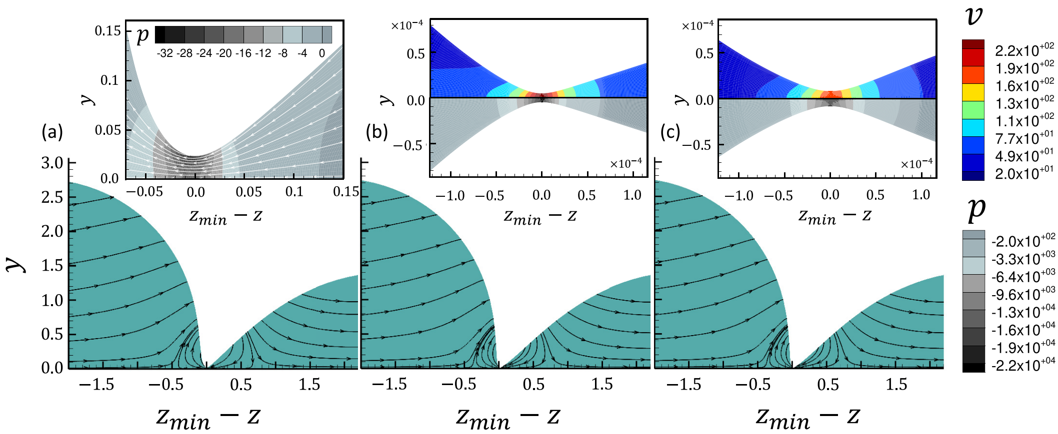

FIG. 3. Computed profiles of and instantaneous streamlines and lateral velocity v and pressure p contours within a 2D drop of $\mathrm{Oh} = 10^{-4}$ and $L_0 = 100$ near the instant in time when it escapes from pinch-off. In this and the next figure, time increases from left to right. The three main figures in (a)–(c) show the interface shapes of and the instantaneous streamlines within the 2D drop. Insert to (a) is a zoomed in view of the location $z_{\min}$ where the sheet half-thickness is a minimum $h_{\min}$ that shows the streamlines and pressure contours (contour values of the pressure are shown by the legend in the insert). Inserts to (b) and (c) are zoomed in views of the pinch region that show contours of lateral velocity v for $y > 0$ and contours of pressure p for $y < 0$ (contour values of both are shown by the legend on the right side of the figure). As $|v| \gg |u|$ in the neck region, the contours obtained from simulations indeed show that $|p| \sim \frac{1}{2}|\mathbf{v}|^2 \approx \frac{1}{2}v^2$ as discussed in the text. In both this figure and the next one, the times at which subplots (b) and (c) are shown have been chosen so that the ratio of $h_{\min}$ at the advanced time, $h_{\min}|_{(c)}$, to that at the earlier time, $h_{\min}|_{(b)}$, is about the same for both values of Oh. Specifically, $h_{\min}|_{(c)}/h_{\min}|_{(b)} \approx 1.69$. Here the minimum sheet half-thickness in panel (b) $h_{\min}|_{(b)} = 4.796 \times 10^{-6}$ and that in panel (c) $h_{\min}|_{(3)} = 8.111 \times 10^{-6}$.

not vary with Oh and where $h^*_{\min} \sim \mathrm{Oh}^2$ and another at still small but larger values of Oh where t^* decreases as Oh increases and $h^*_{\min} \sim \mathrm{Oh}^{1/2}$.

In order to uncover the nature of the mechanisms of escape from pinch-off in these two scaling regimes, we next investigate the transient evolution of the flow and pressure fields within the contracting sheets (Figs. 3 and 4) and provide simple scaling arguments to rationalize the differences

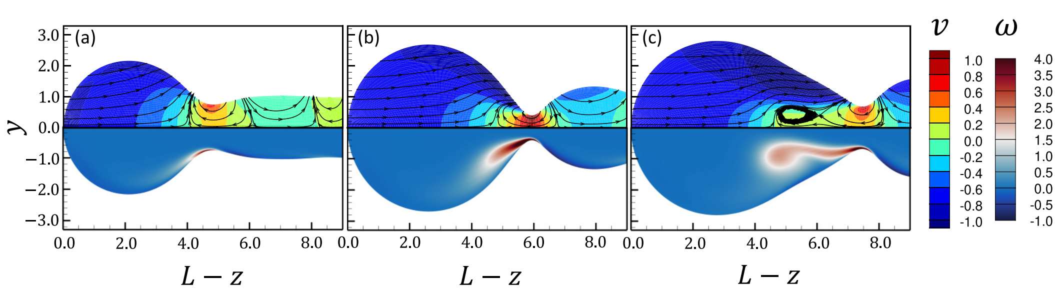

FIG. 4. Computed profiles of and instantaneous streamlines and lateral velocity v and vorticity ω contours within a 2D drop of $\mathrm{Oh} = 10^{-2}$ and $L_0 = 100$ near the instant in time when it escapes from pinch-off. In all frames, streamlines and contours of lateral velocity v are shown for $y > 0$ and contours of vorticity ω are shown for $y < 0$. Contour values of both are indicated by the legend on the right side of the figure. Here the minimum sheet half-thickness in panel (b) $h_{\min}|_{(b)} = 0.4083$ and that in panel (c) $h_{\min}|_{(c)} = 0.6892$.

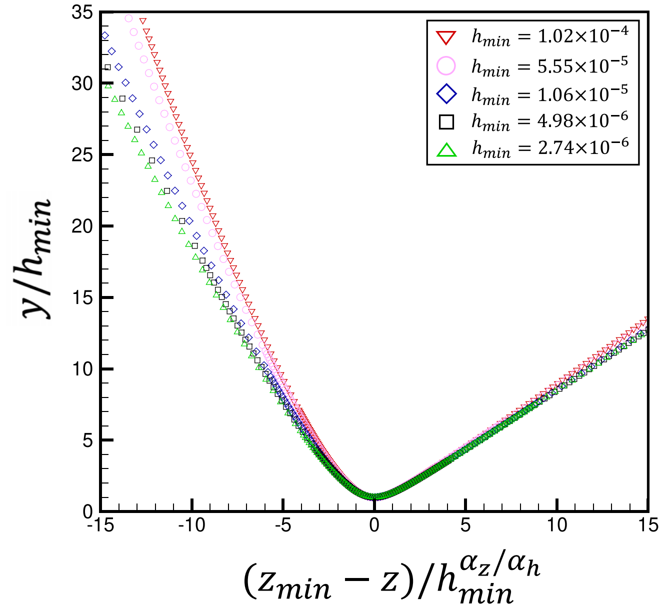

FIG. 5. Suitably rescaled interface shapes in the vicinity of the location where the sheet half-thickness is a minimum, viz. $(y, z) = (h_{\min}, z_{\min})$, obtained from 2D simulations show the collapse of the shapes onto the inviscid similarity profile as $h_{\min}$ decreases. However, as $h_{\min}$ continues to decrease, viscous resistance in the thinning sheet becomes important, and the interface shapes begin to depart from the self-similar profile as the neck starts to reopen and the sheet escapes from pinch-off. Here $\mathrm{Oh} = 5 \times 10^{-5}$ and $L_0 = 100$.

in the responses observed in the simulations first in the quadratic regime (Fig. 3) and then in the square-root regime (Fig. 4).

Figure 3 shows that at early times after the neck has formed and in the vicinity of which the curvature and hence the pressure are negative, fluid is being driven from the region far from the tip toward the tip. If the sheet were an inviscid fluid, then it would be appropriate to tackle the problem using potential flow analysis as in Ref. [26]. In a potential flow, the vorticity vector $\boldsymbol{\omega} \equiv \boldsymbol{\nabla} \times \mathbf{v} = \mathbf{0}$. Thus, $\mathbf{v} = \boldsymbol{\nabla}\phi$ (ϕ: velocity potential) and the continuity and Navier-Stokes equations reduce to Laplace's equation $\nabla^2\phi = 0$ and Bernoulli's equation $\partial\phi/\partial t + (1/2)|\mathbf{v}|^2 + p = 0$ [45]. Thus, balancing the kinetic energy (per unit mass) and the pressure terms, when p falls $|\mathbf{v}|$ rises or when $|\mathbf{v}|$ rises p falls: As the neck of the inviscid 2D drop continues to thin, the magnitude of the fluid velocity rises, and as the magnitude of the fluid velocity continues to rise, the pressure at the neck becomes even more negative. As the pressure becomes more negative, the curvature at the neck has to become more negative to satisfy the traction BC [cf. Eq. (4) which, for inviscid flow, reduces to $-p = 2\mathcal{H}$]. Prior to escape, the simulation results shown in Fig. 3 for a drop of $\mathrm{Oh} \to 0$ accord with results obtained from analyzing the dynamics using potential flow theory. Burton and Taborek [26] have shown that in the vicinity of the location where the neck thickness is a minimum, the dynamics is self-similar: The minimum neck half-thickness $h_{\min} \sim \tau^{\alpha_h}$ and the lateral extent of the pinching zone $L_z \sim \tau^{\alpha_z}$, where the two scaling exponents are given by $\alpha_h = 0.7476$ and $\alpha_z = 0.6869$ and $\tau \equiv t_R - -t$ is the time remaining until pinch-off (t_R: pinch-off time). Figure 5 shows that prior to escape, interface shapes computed from simulations when $\mathrm{Oh} \to 0$ collapse onto a similarity profile with values of the scaling exponents computed from the 2D simulations that are identical to ones obtained from the potential flow simulations of Ref. [26].

As $\alpha_h > \alpha_z$, interface shapes in the vicinity of the minimum neck thickness are slender. Therefore, the local dynamics can be described by means of the slender-sheet equations. As summarized in Appendix A, such a study was carried out in Ref. [26] in the inviscid limit and the authors showed that the scaling exponents resulting from the slender-sheet analysis are identical to those obtained from the potential flow analysis. However, examination of the terms in the full 1D momentum equation as $\tau \to 0$ reveals that the rate of growth of the viscous term, which is neglected in the inviscid analysis, is larger than the rate at which the inertial and surface tension terms in that equation are blowing up. Therefore, neglect of viscous effects is asymptotically incorrect. Indeed, as shown in Appendix A, during thinning of a low-viscosity sheet, the local Reynolds number becomes of order one when $h_{\min} \sim \mathrm{Oh}^2$. Therefore, the scaling of $h_{\min}$ with Oh obtained from this simple scaling argument is identical to the scaling relation predicted from the full 2D free surface flow simulations in Fig. 2 when $\mathrm{Oh} \to 0$. While it is now clear that the escape from pinch-off in the low Oh limit where $h^*_{\min} \sim \mathrm{Oh}^2$ is due to viscous resistance that ultimately becomes sufficiently important in a thinning sheet no matter how small the fluid's viscosity, the reason behind the existence of the second scaling regime that arises at higher Oh is still not known but is addressed in the next paragraph.

When the sheet fluid is still slightly viscous but the Ohnesorge number is not vanishingly small, the simulation results shown in Fig. 4 make plain that the dynamics in the vicinity of the neck of the 2D drop when $\mathrm{Oh} = 10^{-2}$ drastically differs from that when $\mathrm{Oh} = 10^{-4}$ (Fig. 3) and that the drop of larger Oh escapes from pinch-off at a larger value of the minimum neck half-thickness than the drop of smaller Oh [Figs. 2(b) and 3]. In the case of the contracting 2D drop discussed in the previous paragraph, the dynamics when $\mathrm{Oh} = 10^{-4}$ is virtually identical to that of a drop of an inviscid fluid undergoing potential flow until the minimum thickness of the neck has become sufficiently small for viscous resistance to become important, and leads to the reopening of the neck and escape from pinch-off. However, Fig. 4 shows that unlike the potential flow-like dynamics observed with the drop of $\mathrm{Oh} = 10^{-4}$, vorticity plays a significant role when $\mathrm{Oh} = 10^{-2}$. In a 2D flow in the yz plane, the vorticity vector $\boldsymbol{\omega} = \nabla \times \mathbf{v}$ only has a nonzero component in the x direction which is hereafter denoted by $\omega \equiv [\nabla \times \mathbf{v}]_x$ and simply referred to as the vorticity. In such a 2D flow, the evolution in time of vorticity in the flow domain is governed by the scalar vorticity transport equation [46]

$$\frac{D\omega}{Dt} \equiv \frac{\partial \omega}{\partial t} + \mathbf{v} \cdot \nabla \omega = \mathrm{Oh}\, \nabla^2 \omega. \tag{7}$$

During drop recoil, the free surface of the drop is a source of vorticity. As the 2D drop contracts, a substantial amount of vorticity is generated by the motion of the highly curved interface and is transported from the free surface into the interior of the drop. Integration of the vorticity transport equation over the drop's volume $V(t)$ yields

$$\frac{D}{Dt} \int_{V(t)} \omega dV = \mathrm{Oh} \int_{S(t)} \mathbf{n} \cdot \nabla \omega \, ds = -2\mathrm{Oh} \int_{S(t)} \mathbf{n} \cdot \nabla \left(\frac{\partial v_n}{\partial s} + (2\mathcal{H}) v_t \right) ds, \tag{8}$$

where $v_n \equiv \mathbf{n} \cdot \mathbf{v}$ and $v_t \equiv \mathbf{t} \cdot \mathbf{v}$ are the components of the fluid velocity in the normal and tangential directions to $S(t)$, s denotes arc length along the interface, and the derivation of the expression for the vorticity at the surface of the 2D drop—the surface vorticity—that has been used in going from the first to the second integral along the free surface is shown in Appendix B. Thus, the rate at which vorticity is generated and then transported into the the drop from its free surface [cf. Eq. (8)] and subsequently the rate at which that vorticity diffuses into the drop's interior [cf. Eq. (7)] increase as Oh increases. Therefore, in order for vorticity to affect whether the thinning neck of a low-viscosity drop will pinch-off or escape from pinch-off, the timescale for vorticity transport, i.e., the timescale for vorticity that has been generated at the free surface to have significantly penetrated the region in the neighborhood of the thinning neck, $\tilde{t}_w \equiv \rho \tilde{h}^2_{\min}/\mu$, should be comparable to the timescale for inertial-capillary pinch-off, $\tilde{t}_{ic} = (\rho \tilde{h}_0^3/\sigma)^{1/2}$. Equating these two timescales yields the simple scaling law that $h_{\min} \sim \mathrm{Oh}^{1/2}$, a result which accords with the simulation results reported in Fig. 2(b). As shown in frame (a) of Fig. 4, initially vorticity is confined to a thin layer adjacent to the free surface. However, as shown in frame (b) of Fig. 4, at a later time when the neck has further thinned, there is now significant penetration of vorticity into the 2D drop in the neighborhood of the neck. Yet later, as shown in frame (c) of Fig. 4, a vortex has detached from the free surface, resulting

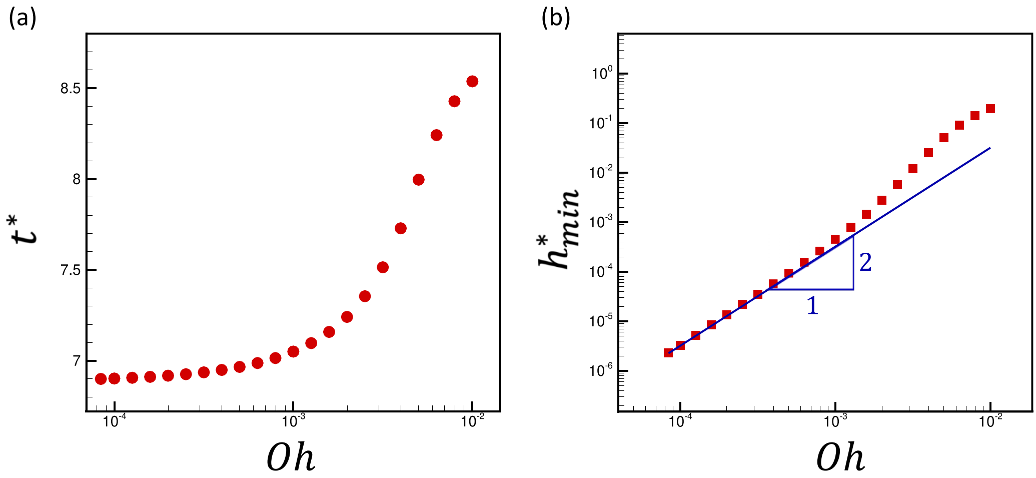

FIG. 6. The computed variation with Ohnesorge number Oh of (a) the time t^* and (b) the minimum value of the sheet half-thickness $h^*_{\min}$ at which the neck of a recoiling liquid sheet or a 2D drop stops thinning and the sheet escapes from pinch-off that has been obtained from simulations in which the 1D slender-sheet equations have been solved. In both (a) and (b), simulation results are denoted by the red symbols. In (b), the blue line of slope 2 denotes the theoretical scaling law $h^*_{\min} \sim \mathrm{Oh}^2$. Here $L_0 = 100$.

in a flow that is directed from the bulbous tip toward the neck, causing the neck thickness to begin to increase and for the 2D drop to escape from pinch-off.

VI. 1D RESULTS

Paralleling the analyses and results presented in the previous section, the contraction dynamics of low-viscosity 2D drops has been studied using the slender-sheet equations. As in the 2D analysis, simulations using the 1D slender-sheet equations also show that even a minute amount of viscosity will prevent pinch-off during the retraction of liquid sheets. As in Sec. V, after the elapse of time t^* from the beginning of contraction and when the minimum value of the sheet half-thickness $h_{\min}$ has fallen to an extremely small value $h^*_{\min} \ll 1$, the sheet once again escapes from breakup. However, Fig. 6 shows that according to the 1D results, there is only one scaling regime of escape from pinch-off and in that regime $h^*_{\min} \sim \mathrm{Oh}^2$.

The fact that the analysis based on the slender-sheet equations only predicts the quadratic scaling regime due to viscous resistance could have been anticipated a priori because in slender-sheet theory the flow field is vorticity free to leading order. In slender-sheet analysis, the dominant lateral or horizontal component of velocity v is independent of the vertical coordinate y, viz. $v = v(z, t)$, and the vertical component of velocity $u \ll v$ and is of order y. Hence, vorticity is of order y or small in slender-sheet theory, thereby precluding the possibility of vorticity-driven escape from pinch-off when the dynamics is analyzed using the 1D equations.

VII. CONCLUSIONS

In this paper, the contraction dynamics of highly elongated 2D drops, which approximate well cross sections of liquid sheets, has been analyzed by means of both 2D free surface flow simulations and 1D simulations based on solving the slender-sheet equations. When the fluid is inviscid, Burton and Taborek [26] have shown that a slender 2D drop whose two ends contract toward each other due the difference in the surface tension (capillary) pressure between its two rounded ends and its central portion (consisting of a region of fluid bound by two flat, parallel surfaces) can pinch-off even in the absence of van der Waals forces. The dynamics in the vicinity of the singularity for the inviscid 2D drop is self-similar. According to the foregoing results, for small yet finite viscosity μ, a contracting liquid sheet or a 2D drop will escape from pinch-off when van der Waals forces are absent. By means of 2D free surface flow simulations, the escape from pinch-off is shown to occur due to two different mechanisms attributable to finite viscosity. For extremely small viscosities or, more precisely, for $\mathrm{Oh} \equiv \mu/\sqrt{\rho\sigma\tilde{h}_0} \to 0$, escape is shown to be due to viscous resistance. For somewhat larger but yet still small viscosities or Oh, the escape occurs for values of the minimum sheet thickness that are much larger than those when $\mathrm{Oh} \to 0$ and can be attributed to vorticity generation at the free surface. In the former case, the value of the minimum sheet half-thickness $h^*_{\min}$ for which escape occurs that is obtained from 2D free surface flow simulations is shown to follow the scaling relation $h^*_{\min} \sim \mathrm{Oh}^2$ and in the latter case the minimum sheet half-thickness for escape from such simulations is shown to scale as $h^*_{\min} \sim \mathrm{Oh}^{1/2}$. These two relations obtained from the 2D simulations have been shown to accord with theoretical estimates deduced from simple scaling arguments.

In this paper, the breakup of liquid sheets has also been analyzed using 1D simulations based on the slender-sheet equations. The results of such simulations show that the value of the minimum sheet half-thickness for which escape occurs follows the scaling relation $h^*_{\min} \sim \mathrm{Oh}^2$. That only the quadratic scaling regime due to viscous resistance is predicted from the slender-sheet analysis accords with expectation because the slender-sheet formulation is vorticity free to leading order. As the lateral velocity v to leading order is locally plug-flow or independent of the vertical coordinate y, viz. $v = v(z, t)$, and the vertical velocity u is of order y, vorticity is of order y or small in slender-sheet theory. Hence, a fully 2D theory is needed to determine the dynamics at any Oh and predict both scaling regimes.

It is also worth mentioning that there have been other studies of 2D pinch-off aside from the work of Burton and Taborek [26]. It should be emphasized, however, that all of these studies have relied on the use of 1D slender-sheet equations and hence the lubrication approximation. Especially noteworthy among such studies is the paper by Dupont *et al.* [47] on finite time singularity formation in Hele-Shaw cells in which the authors used a viscous term that is linearly proportional to velocity. However, as demonstrated in Appendix A of our paper, this simplified linear form of the viscous force would fail to keep pace with surface tension force and inertia as $\tau \to 0$. Consequently, as has already been noted by Burton and Taborek [26], the breakup dynamics would be self-similar and adhere to the scaling laws determined by Burton and Taborek. Moreover, the adoption of the linear form of the viscous force would preclude the possibility of escape from pinch-off.

Also noteworthy in studies of 2D pinch-off in Hele-Shaw systems is the manner in which an external pressure is imposed. In their studies of Hele-Shaw flow with zero fluid density, Dupont *et al.* [47,48] demonstrated that a thin sheet can rupture in finite and/or infinite time depending on how the external pressure is imposed. However, these authors did not investigate this effect for flow with finite fluid density which is more relevant for our work. Regardless, it should be noted that in the paper by Dupont *et al.* [47], external pressure appears only as a boundary condition and not in the equations governing the dynamics of the sheet. Therefore, if the effect of finite viscosity is accounted for in the asymptotically consistent form, i.e., as $\frac{\partial^2 v}{\partial z^2}$, then the sheet will indeed escape from pinch-off. Here the escape occurs because an imposed time-dependent pressure acts solely as a boundary condition and does not influence the reopening dynamics which is purely localized and independent of boundary conditions. In summary, while altering the externally imposed pressure would affect the global dynamics, it would have no effect whatsoever on the localized reopening dynamics.

According to the results presented in this paper and as has been summarized in the first paragraph of this section, the dimensionless minimum sheet half-thickness $h^*_{\min}$ for which escape from pinch-off occurs follows one of two scaling laws: for extremely small viscosities or for $\mathrm{Oh} \equiv \mu/\sqrt{\rho\sigma\tilde{h}_0} \to 0$, $h^*_{\min} \equiv \tilde{h}_{\min}/\tilde{h}_0 \sim \mathrm{Oh}^2$, whereas for somewhat larger but yet still small viscosities or small Oh, $h^*_{\min} \sim \mathrm{Oh}^{1/2}$. We note that aside from being the ratio of viscous stress to the square root of the product of inertial and capillary stresses, the Ohnesorge number also equals the square root of the ratio of the viscous length $\tilde{l}_\mu \equiv \mu^2/(\rho\sigma)$ to the initial sheet half-thickness $\tilde{h}_0$:

$$\mathrm{Oh} \equiv \frac{\mu}{(\rho\sigma\tilde{h}_0)^{1/2}} = \left(\frac{\mu^2}{\rho\sigma}\frac{1}{\tilde{h}_0}\right)^{1/2} = \left(\frac{\tilde{l}_\mu}{\tilde{h}_0}\right)^{1/2}. \tag{9}$$

Therefore, in the former or quadratic scaling regime, which is attained when viscous force has become comparable to inertia and surface tension force, the dimensional minimum sheet half-thickness $\tilde{h}^*_{\min} \sim \tilde{l}_\mu$. It is worth noting that this is identically the intrinsic length scale, i.e., the length scale for which viscous force is comparable to inertia and surface tension force, in 3D pinch-off of liquid drops, jets, and filaments [41,49–53]. At room temperature, $\tilde{l}_\mu \approx 14$ nm if the working liquid is water. Since van der Waals force would become important when the sheet half-thickness becomes of the order of one hundred nanometers, a thinning liquid sheet of water would succumb to it and tend toward rupture long before viscous force could become sufficiently large to enable the sheet to escape from pinch-off. If, however, the working liquid is a 60% glycerol-water solution that is about 10 times more viscous than water, then $\tilde{l}_\mu \approx 1400$ nm or 1.4 µm [54]. In this situation, the liquid sheet would be able to escape pinch-off before it could become sufficiently thin for van der Waals force to become operative.

The analyses reported in this paper can be extended in a number of fruitful directions. Among others, it would be highly desirable in future research efforts to analyze the dynamics of contraction of 2D drops for systems containing both insoluble [18,55] and soluble surfactants [56]. For both practical and scientific reasons, it would be equally valuable in future work to address the dynamics of contraction of 2D drops when the fluid is non-Newtonian [57] rather than a simple Newtonian fluid as in this paper.

ACKNOWLEDGMENTS

The authors thank the Purdue Process Safety and Assurance Center (P2SAC) and the Purdue Multiphase Flow Center (PMULFLOW), and the Burton and Kathryn Gedge Professorship to O.A.B. for financial support.

The authors report no conflict of interest.

APPENDIX A: SLENDER-SHEET EQUATIONS: INVISCID LIMIT AND EFFECT OF SMALL VISCOSITY

Burton and Taborek [26] have shown by solving the slender-sheet equations for a liquid sheet of an inviscid fluid, i.e., when $\mathrm{Oh} = 0$, that the dynamics in the vicinity of the location where the neck thickness is a minimum is self-similar. In this situation, the minimum neck half-thickness $h_{\min} \sim \tau^{\alpha_h}$ and the lateral extent of the pinching zone $L_z \sim \tau^{\alpha_z}$ where the two scaling exponents are given by $\alpha_h = 0.7476$ and $\alpha_z = 0.6869$ and $\tau \equiv t_R - t$ is the time remaining until pinch-off (t_R: pinch-off time). Using these values of the scaling exponents, it follows that the inertial and the surface tension terms in the 1D momentum equation (6) blow up as $\tau \to 0$ as:

$$\frac{\partial v}{\partial t} \sim v\,\frac{\partial v}{\partial z} \sim \tau^{\alpha_z - 2} \equiv \tau^{-1.3131} \quad \text{and} \quad \frac{\partial^3 h}{\partial z^3} \sim \tau^{\alpha_h - 3\alpha_z} \equiv \tau^{-1.3131} \tag{A1}$$

However, using the values of these scaling exponents to estimate the variation with τ of the viscous term when Oh is small but nonzero yields that

$$4\frac{\mathrm{Oh}}{h}\frac{\partial}{\partial z}\left(h\,\frac{\partial v}{\partial z}\right) \sim \mathrm{Oh}\,\tau^{-\alpha_z - 1} \equiv \mathrm{Oh}\,\tau^{-1.6869}. \tag{A2}$$

Comparison of the inertial and surface tension terms [Eq. (A1)] with the viscous term [Eq. (A2)] reveals that the rate at which the viscous term is growing as $\tau \to 0$ is larger than the rates at which the other two terms are growing as the sheet thins. Therefore, as the viscous term is multiplied by Oh, it is initially, i.e., for values of τ that are of order one or larger, much smaller than the other two terms when $\mathrm{Oh} \ll 1$, it eventually catches up to the other two terms. Hence, the neglect of the viscous term is asymptotically inconsistent. By either equating the viscous term which was assumed to be negligible with the other two terms or, equivalently, calculating the time at which the local Reynolds number in the vicinity of the minimum neck thickness becomes of order one, it can be shown that the viscous term becomes comparable to the inertial and the surface tension terms when $h_{\min} \sim \mathrm{Oh}^{\alpha_h/(2\alpha_z-1)} \equiv \mathrm{Oh}^2$.

APPENDIX B: VORTICITY AT A FREE SURFACE

In a 2D flow in the yz plane, the vorticity $\omega = \mathbf{e}_x \cdot (\nabla \times \mathbf{v})$. At the free surface $S(t)$ of the 2D drop, the unit normal and tangent to $S(t)$ can be used to write $\mathbf{e}_x = \mathbf{n} \times \mathbf{t}$. Therefore, the vorticity at the free surface—the surface vorticity—can be expressed as

$$\begin{aligned}
\omega &= (\mathbf{n} \times \mathbf{t}) \cdot (\nabla \times \mathbf{v}) = [\mathbf{n} \times \mathbf{t}]_i [\nabla \times \mathbf{v}]_i \\
&= \epsilon_{ijk} [\mathbf{n}]_j [\mathbf{t}]_k \, \epsilon_{imn} [\nabla]_m [\mathbf{v}]_n \\
&= (\delta_{jm}\delta_{kn} - \delta_{jn}\delta_{km}) [\mathbf{n}]_j [\mathbf{t}]_k [\nabla]_m [\mathbf{v}]_n \\
&= [\mathbf{n}]_m [\mathbf{t}]_n [\nabla]_m [\mathbf{v}]_n - [\mathbf{n}]_n [\mathbf{t}]_m [\nabla]_m [\mathbf{v}]_n \\
&= \mathbf{n} \cdot \nabla \mathbf{v} \cdot \mathbf{t} - \mathbf{t} \cdot \nabla \mathbf{v} \cdot \mathbf{n},
\end{aligned} \tag{B1}$$

where δ_{ij} is the Kronecker delta, ϵ_{ijk} is the permutation symbol, and single subscripts refer to components of vectors, and use has been made of the Einstein summation convention. To make further progress, we make use of the tangential component of the traction BC or the vanishing of the shear stress at the interface, viz. $\mathbf{n} \cdot \mathbf{T} \cdot \mathbf{t} = 0$. This condition can be expressed as

$$\mathbf{n} \cdot \nabla \mathbf{v} \cdot \mathbf{t} + \mathbf{t} \cdot \nabla \mathbf{v} \cdot \mathbf{n} = 0. \tag{B2}$$

Using (B2), one can rewrite (B1) as $\omega = -2\mathbf{t} \cdot \nabla \mathbf{v} \cdot \mathbf{n}$. It then follows that the vorticity at the free surface can be expressed in terms of the normal and tangential components of the fluid velocity at $S(t)$:

$$\begin{aligned}
\omega &= -2\mathbf{t} \cdot \nabla \mathbf{v} \cdot \mathbf{n} = -2\frac{\partial \mathbf{v}}{\partial s} \cdot \mathbf{n} \\
&= -2\left[\frac{\partial}{\partial s}(\mathbf{v} \cdot \mathbf{n}) - \mathbf{v} \cdot \frac{\partial \mathbf{n}}{\partial s}\right] \\
&= -2\left[\frac{\partial v_n}{\partial s} - v_t \mathbf{t} \cdot \frac{\partial \mathbf{n}}{\partial s}\right].
\end{aligned} \tag{B3}$$

In a 2D flow, $-2\mathcal{H} = \nabla_s \cdot \mathbf{n} = \mathbf{t} \cdot \frac{\partial \mathbf{n}}{\partial s}$ where $\nabla_s = (\mathbf{I} - \mathbf{n}\mathbf{n}) \cdot \nabla$. Therefore, the surface vorticity can be written as

$$\omega = -2\left[\frac{\partial v_n}{\partial s} + (2\mathcal{H}) v_t\right] \tag{B4}$$

In Sec. V, this expression for ω is used to simplify the surface integral on the first line of Eq. (8) into its final form on the second line of that equation.

[1] L. P. Bayvel and Z. Orzechowski, *Liquid Atomization* (CRC Press, Boca Raton, FL, 1993)
[2] A. H. Lefebvre and V. G. McDonell, *Atomization and Sprays* (CRC Press, Boca Raton, FL, 2017).
[3] S. Middleman, *Fundamentals of Polymer Processing* (McGraw–Hill College, New York, 1977).

[4] L. Rayleigh, XIX. On the instability of cylindrical fluid surfaces, Phil. Mag. **34**, 177 (1892).
[5] J. Plateau, *Experimental and theoretical statics of liquids subject to molecular forces only* (Gauthier-Villars, Paris, 1873), Vol. 4.
[6] P.-G. de Gennes, Wetting: Statics and dynamics, Rev. Mod. Phys. **57**, 827 (1985).
[7] G. F. Teletzke, H. T. Davis, and L. E. Scriven, How liquids spread on solids, Chem. Engng. Commun. **55**, 41 (1987).
[8] A. Sheludko, Certain peculiarities of foamlamellas, Parts I–III, in *Proc. Koninkl. Ned. Akad. Wetenschap. B*, (1962), Vol. 65, pp. 76–108.
[9] A. Vrij, Possible mechanism for the spontaneous rupture of thin, free liquid films, Discuss. Faraday Soc. **42**, 23 (1966).
[10] A. Sheludko, Thin liquid films, Advan. Colloid Interface Sci. **1**, 391 (1967).
[11] E. Ruckenstein and R. K. Jain, Spontaneous rupture of thin liquid films, J. Chem. Soc. Faraday Trans. 2 **70**, 132 (1974).
[12] D. Vaynblat, J. R. Lister, and T. P. Witelski, Rupture of thin viscous films by van der waals forces: Evolution and self-similarity, Phys. Fluids **13**, 1130 (2001).
[13] G. I. Barenblatt, *Scaling, Self-similarity, and Intermediate Asymptotics: Dimensional Analysis and Intermediate Asymptotics*, Cambridge Texts in Applied Mathematics (Cambridge University Press, Cambridge, UK, 1996).
[14] M. P. Ida and M. J. Miksis, Thin film rupture, Appl. Math. Lett. **9**, 35 (1996).
[15] S. S. Thete, C. Anthony, P. Doshi, M. T. Harris, and O. A. Basaran, Self-similarity and scaling transitions during rupture of thin free films of Newtonian fluids, Phys. Fluids **28**, 092101 (2016).
[16] S. S. Thete, C. Anthony, O. A. Basaran, and P. Doshi, Self-similar rupture of thin free films of power-law fluids, Phys. Rev. E **92**, 023014 (2015).
[17] M. S. Bazzi and M. S. Carvalho, Effect of viscoelasticity on liquid sheet rupture, J. Non-Newtonian Fluid Mech. **264**, 107 (2019).
[18] H. Wee, B. W. Wagoner, and O. A. Basaran, Spontaneous rupture of surfactant-covered thin liquid sheets, Phys. Rev. Fluids **7**, 094005 (2022).
[19] V. Garg, S. S. Thete, C. R. Anthony, and O. A. Basaran, Local dynamics during thinning and rupture of liquid sheets of power-law fluids, J. Fluid Mech. **942**, A15 (2022).
[20] G. I. Taylor, The dynamics of thin sheets of fluid. III. Disintegration of fluid sheets, Proc. R. Soc. Lond. **253**, 313 (1959).
[21] F. E. C. Culick, Comments on a ruptured soap film, J. Appl. Phys. **31**, 1128 (1960).
[22] M. P. Brenner and D. Gueyffier, On the bursting of viscous films, Phys. Fluids **11**, 737 (1999).
[23] G. Sünderhauf, H. Raszillier, and F. Durst, The retraction of the edge of a planar liquid sheet, Phys. Fluids **14**, 198 (2002).
[24] N. Savva and J. W. M. Bush, Viscous sheet retraction, J. Fluid Mech. **626**, 211 (2009).
[25] H. Deka and J.-L. Pierson, Revisiting the Taylor-Culick approximation. II. Retraction of a viscous sheet, Phys. Rev. Fluids **5**, 093603 (2020).
[26] J. C. Burton and P. Taborek, Two-dimensional inviscid pinch-off: An example of self-similarity of the second kind, Phys. Fluids **19**, 102109 (2007).
[27] M. A. Fontelos, G. Kitavtsev, and R. M. Taranets, Asymptotic decay and non-rupture of viscous sheets, Z. Angew. Math. Phys. **69**, 79 (2018).
[28] X. Zhang, R. S. Padgett, and O. A. Basaran, Nonlinear deformation and breakup of stretching liquid bridges, J. Fluid Mech. **329**, 207 (1996).
[29] B. Ambravaneswaran, S. D. Phillips, and O. A. Basaran, Theoretical analysis of a dripping faucet, Phys. Rev. Lett. **85**, 5332 (2000).
[30] B. Ambravaneswaran, H. J. Subramani, S. D. Phillips, and O. A. Basaran, Dripping-jetting transitions in a dripping faucet, Phys. Rev. Lett. **93**, 034501 (2004).
[31] B. Ambravaneswaran, E. D. Wilkes, and O. A. Basaran, Drop formation from a capillary tube: Comparison of one-dimensional and two-dimensional analyses and occurrence of satellite drops, Phys. Fluids **14**, 2606 (2002).

[32] X. Liu, B. W. Wagoner, H. Wee, and O. A. Basaran, Effect of initial conditions on promotion and inhibition of breakup during filament contraction, AIChE J. **68**, e17491 (2022).
[33] X. Liu, B. W. Wagoner, and O. A. Basaran, Contraction velocity of viscoelastic filaments, Phys. Rev. Fluids **7**, L121601 (2022).
[34] M. S. Gockenbach, *Understanding and Implementing the Finite Element Method* (SIAM, Philadelphia, PA, 2006).
[35] P. M. Gresho, R. L. Lee, and R. C. Sani, in *Recent Advances Numerical Methods in Fluids*, edited by C. Taylor and K. Morgan (Pineridge, Swansea, 1980), pp. 27–79.
[36] N. E. Bixler, An improved time integrator for finite element analysis, Commun. App. Numer. Methods **5**, 69 (1989).
[37] K. N. Christodoulou and L. E. Scriven, Discretization of free surface flows and other moving boundary problems, J. Comput. Phys. **99**, 39 (1992).
[38] P. K. Notz and O. A. Basaran, Dynamics and breakup of a contracting liquid filament, J. Fluid Mech. **512**, 223 (2004).
[39] R. Suryo, P. Doshi, and O. A. Basaran, Nonlinear dynamics and breakup of compound jets, Phys. Fluids **18**, 082107 (2006).
[40] R. Suryo and O. A. Basaran, Dripping of a liquid from a tube in the absence of gravity, Phys. Rev. Lett. **96**, 034504 (2006).
[41] J. R. Castrejón-Pita, A. A. Castrejón-Pita, S. S. Thete, K. Sambath, I. M. Hutchings, J. Hinch, J. R. Lister, and O. A. Basaran, Plethora of transitions during breakup of liquid filaments, Proc. Natl. Acad. Sci. USA **112**, 4582 (2015).
[42] H. Wee, C. R. Anthony, and O. A. Basaran, Breakup of a low-viscosity liquid thread, Phys. Rev. Fluids **7**, L112001 (2022).
[43] C. R. Anthony, H. Wee, V. Garg, S. S. Thete, P. M. Kamat, B. W. Wagoner, E. D. Wilkes, P. K. Notz, A. U. Chen, R. Suryo, K. Sambath, J. C. Panditaratne, Y.-C. Liao, and O. A. Basaran, Sharp interface methods for simulation and analysis of free surface flows with singularities: Breakup and coalescence, Annu. Rev. Fluid Mech. **55**, 707 (2023).
[44] Ö. E. Yıldırım and O. A. Basaran, Dynamics of formation and dripping of drops of deformation-rate-thinning and-thickening liquids from capillary tubes, J. Non-Newton. Fluid Mech. **136**, 17 (2006).
[45] L. D. Landau and E. M. Lifshitz, *Fluid Mechanics* (Pergamon Press, Oxford, 1987), Vol. 6.
[46] W. M. Deen, *Analysis of Transport Phenomena* (Oxford University Press, New York, 1998).
[47] T. F. Dupont, R. E. Goldstein, L. P. Kadanoff, and S.-M. Zhou, Finite-time singularity formation in hele-shaw systems, Phys. Rev. E **47**, 4182 (1993).
[48] P. Constantin, T. F. Dupont, R. E. Goldstein, L. P. Kadanoff, M. J. Shelley, and S.-M. Zhou, Droplet breakup in a model of the Hele-Shaw cell, Phys. Rev. E **47**, 4169 (1993).
[49] J. Eggers, Universal pinching of 3D axisymmetric free-surface flow, Phys. Rev. Lett. **71**, 3458 (1993).
[50] X. D. Shi, M. P. Brenner, and S. R. Nagel, A cascade of structure in a drop falling from a faucet, Science **265**, 219 (1994).
[51] J. R. Lister and H. A. Stone, Capillary breakup of a viscous thread surrounded by another viscous fluid, Phys. Fluids **10**, 2758 (1998).
[52] O. A. Basaran, Small-scale free surface flows with breakup: Drop formation and emerging applications, AIChE J. **48**, 1842 (2002).
[53] J. Eggers and E. Villermaux, Physics of liquid jets, Rep. Prog. Phys. **71**, 036601 (2008).
[54] M. L. Sheely, Glycerol viscosity tables, Ind. Eng. Chem. **24**, 1060 (1932).
[55] Y. C. Liao, E. I. Franses, and O. A. Basaran, Deformation and breakup of a stretching liquid bridge covered with an insoluble surfactant monolayer, Phys. Fluids **18**, 022101 (2006).
[56] Y.-C. Liao, H. J. Subramani, E. I. Franses, and O. A. Basaran, Effects of soluble surfactants on the deformation and breakup of stretching liquid bridges, Langmuir **20**, 9926 (2004).
[57] R. B. Bird, R. C. Armstrong, and O. Hassager, *Dynamics of Polymeric Liquids, Volume 1: Fluid Mechanics*, 2nd ed. (Wiley, New York, 1987).